Integrated structural and control system design (co-design) for robust flutter suppression

Pilar Tagliero*[1], Emmeline Faïsse[2], and Joseph Morlier[3]

ISAE-SUPAERO, Toulouse, France
[1] *Graduate student*
[2] *Associate research supervisor and doctoral researcher*
[3] *Research supervisor and professor*

Submitted: April 11, 2021

Abstract

Traditional design process consists in designing the physical artifact first and then its control system. However, this approach only produces sub optimal results since the coupling between the two designs is not taken into account. The aim of this work is to perform an integrated structural and control system design for a wing in order to reduce the mass of the system as well as maintaining or improving its flutter performance. The Goland wing with a flap modeled as a cantilever thin-walled beam is considered. A state-feedback controller is used. Ten design variables are optimized: five thicknesses of the thin-walled beam structure, four control gains and the size of the flap. The effect of using different objective functions, models and design variables is explored. Mass reduction benefits are obtained. However, the design lacks of robustness to thickness variations.
Keywords: Co-design, Flutter, MDO

Nomenclature

α	pitch angle
β	flap deflection angle
χ	vector of design variables
κ	structural stiffness matrix
μ	inertia matrix
ω_F	flutter pulsation
ω_α	pitch mode pulsation
ω_h	plunge mode pulsation
ρ	$= 1.225\, kg/m^3$, air density
ρ_m	density of the material of the wing
ε	finite difference step size
ζ	structural damping matrix
b	semichord
c	total chord
c_f	flap chord
c_s	length of the wingbox
c_α	pitch structural damping coefficient
c_h	plunge structural damping coefficient
$C_{L\alpha}$	lift coefficient
$C_{L\beta}$	lift coefficient per flap angle deflected
$C_{M\alpha}$	coefficient of pitch moment about the aerodynamic center
$C_{M\beta}$	coefficient of moment per flap angle deflected
E	Young's modulus
ea_b	position of the elastic axis from the leading edge in fractions of the semichord
EF	ratio of the flap chord with respect to the total chord
G	shear modulus
h	plunge
I_α	mass moment of inertia of the wing section about its elastic axis
I_x	area moment of inertia of the wing section about its horizontal axis
J	torsion constant
K_α	control gain on α
k_α	structural spring constant in pitch
$K_{\dot\alpha}$	control gain on $\dot\alpha$
$K_{\dot h}$	control gain on $\dot h$
K_h	control gain on h
k_h	structural spring constant in plunge
L	aerodynamic lift force
M	aerodynamic moment
m	total mass of the wing model
s	semi-span
t	time
t_0	height of the wing section
$t_1 - t_5$	thicknesses of the wingbox
U	flow speed
V_F	flutter speed
x_α	distance of the center of gravity measured from the elastic axis in fractions of the semichord

1 Introduction

"Aeroelasticity deals with the behavior of an elastic body in an airstream, wherein there is significant reciprocal interaction or feedback between deformation and flow." [1]. Flexible structures are prone to deform under aerodynamic loads. Since these loads depend on the geometry of the structure, the structural deforma-

*pilar-julieta.tagliero@student.isae-supaero.fr

tion changes the aerodynamic loads leading to further distortion and so on [2]. Flutter is a dynamic aeroelastic instability occurring when a particular speed (V_F) is exceeded and consists of violent vibrations of the structure which rapidly increase in amplitude [3], [4]. Nowadays airframe designs tend to be more flexible, slender, and to operate at higher speeds, thus resulting in an increased likelihood of flutter occurrence. As flutter usually causes serious damage on the structure or even its complete destruction, structures must be designed so that the flutter speed is outside the operating speed range and this phenomena is avoided. A classical solution to rise V_F is to increase the structural stiffness, but with the penalty of increasing weight. A most advantageous solution consists in adding to the structure a control system capable of suppressing flutter vibrations [3], [4]. The increase of the capabilities of sensors and actuators has encourage this last solution. In fact, as described in [5], active control systems, such as gust load alleviation systems, are nowadays used in aircraft. However, active flutter suppression systems are not introduced yet due to its complicated certification: a failure could produce catastrophic effects.

The objective of this work is to assess the capability of co-design method to design a wing with an active flutter suppression system. Co-design consists on the simultaneous design of the structure and its control system. Contrary to conventional sequential design (first the plant and then the control) it produces more optimal results by taking into account the coupling between the disciplines [6]. Co-design was applied on the design of an active suspension system in [6] and on the design of a robotic arm in [7]. In [8], by synthesizing the longitudinal/lateral control gains along with the size of the tail, a reduction of 60% of the tail surface was achieved. Co-design was also widely used to suppress vibrations on flexible structures, such as in [9] and [10]. Different publications have addressed the co-design of a wing with flutter constraints considering LQR [11] or H_{inf} [12] techniques. Herein a state-feedback controller on a 2D aeroelastic model is considered.

2 Methodology

The aim of this project is to synthesize a feedback control system in order to suppress flutter instabilities coupled with the structural design of the wing. Consequently, the interaction between the control system and the structure is considered and a system-optimal design is obtained. The co-design is performed using the package SciPy of Python to simplify the future transition to OpenMDAO.

Section 3 describes the aeroelastic model used herein. Ideally, a complete model containing the equations governing the vibration of the elastic wing and the aerodynamic equations describing the motion of the surrounding air should be considered [3]. However, this model would be too complicated to make the control design tractable, even more when the design is made under a multidisciplinary optimization. Being this work a first attempt to assess the feasibility of co-design method, a simple model where the aerodynamic loads are introduced as external forces and moments in the structural equations is used. Section 4 describes the control model: a simple feedback gain loop. Section 5 sets up the optimization problem through the definition of the objective function, design variables, algorithm and constraints. Different problems are addressed. First, a wing model which only considers the aerodynamic effect of the flap (but not its impact on the structure) is used. That is to say, the flap has no mass nor dimension and the wing section is that of Figure 2 with $c_f = t_f = 0$, but it has a contribution on the aerodynamic loads. For this model, name hereafter *section with "ghost" flap*, the co-design is run with two different objectives: first the reduction of mass while maintaining flutter performance, and secondly the reduction of mass as well as enhancement of flutter performance. Five thicknesses and four control gains are optimized. These results are compared with a sequential design: first the structure is optimized and then the controller. Later, the impact of the flap on the structure is considered (name hereafter *section with "real" flap*) and its size is also optimized. In addition, a preliminary assessment of the robustness of the controller to thickness variations is performed. All results are presented and discussed in Section 6. Finally, Section 7 summarizes the conclusions and Section 8, future work proposals to extend the present work.

3 Aeroelastic Model

The wing model is derived from the Goland wing. It consists in a rectangular cantilevered wing with a 20ft span and 6ft chord (Figure 1). Elastic and geometric parameters of the Goland wing are obtained from [13]. The cross-section, constant all over the span, corresponds to a two-cells wingbox with a trailing-edge control surface (Figure 2). The chord of the airfoil (c) equals the sum of the wingbox length (c_s) and the flap portion (c_f). This section is considered to be thin-walled since thin-walled structures are widely used in aeronautics due to their high structural efficiency that addresses the requirement of weight saving.

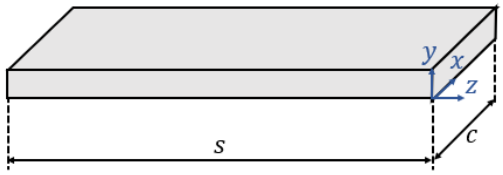

Figure 1: Schema of Goland wing.

The equations of motion correspond to the two-dimensional aeroelastic model presented in Figure 3. In [14] they are shown to be

$$\begin{bmatrix} m & m\,x_\alpha\,b \\ m\,x_\alpha\,b & I_\alpha \end{bmatrix} \begin{bmatrix} \ddot{h} \\ \ddot{\alpha} \end{bmatrix} + \begin{bmatrix} c_h & 0 \\ 0 & c_\alpha \end{bmatrix} \begin{bmatrix} \dot{h} \\ \dot{\alpha} \end{bmatrix} + \\ + \begin{bmatrix} k_h & 0 \\ 0 & k_\alpha \end{bmatrix} \begin{bmatrix} h \\ \alpha \end{bmatrix} = \begin{bmatrix} -L \\ M \end{bmatrix} \quad (1)$$

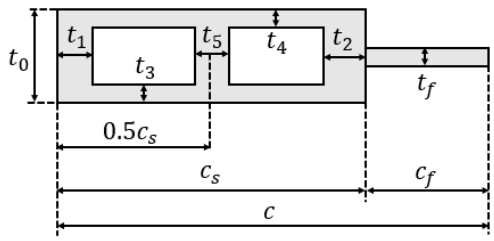

Figure 2: Schema of the wing cross-section. It is composed by a wingbox and an active controlled flap.

or in matrix form

$$\mu \begin{bmatrix} \ddot{h} \\ \ddot{\alpha} \end{bmatrix} + \zeta \begin{bmatrix} \dot{h} \\ \dot{\alpha} \end{bmatrix} + \kappa \begin{bmatrix} h \\ \alpha \end{bmatrix} = \begin{bmatrix} -L \\ M \end{bmatrix} \tag{2}$$

where h and α represent, respectively, the plunge and pitch motion, μ is the inertia matrix, ζ accounts for the structural damping and κ, the structural stiffness.

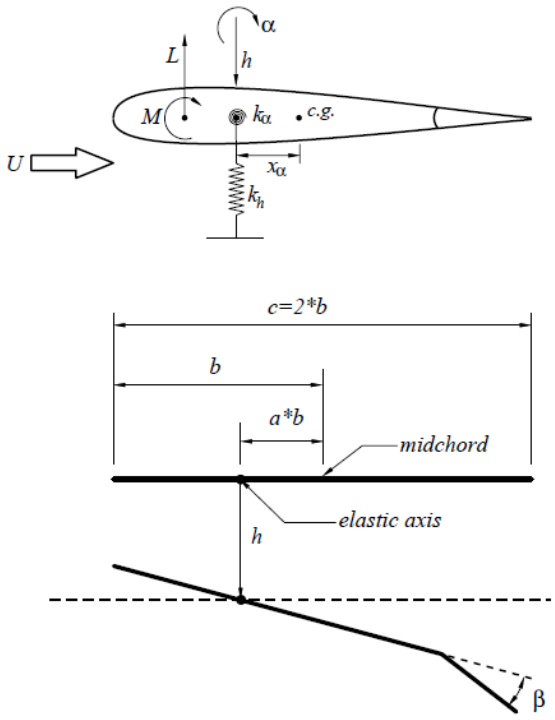

Figure 3: 2D aeroelastic model. The airfoil has two degrees of freedom (pitch and plunge) and a trailing-edgle flap. Reprinted from [14].

The structural spring constants, k_h and k_α are obtained from

$$\omega_h^2 = \frac{k_h}{m} \tag{3}$$

$$\omega_\alpha^2 = \frac{k_\alpha}{I_\alpha} \tag{4}$$

where I_α is the area moment of inertia about the elastic axis of the wing section of Figure 2 and m the mass of the wing.

The damping structural constants, c_h and c_α are estimated as follows (refer to Appendix B for further explanation)

$$c_\alpha = 0.02\sqrt{I_\alpha\, k_\alpha} \tag{5}$$

$$c_h = 0.02\sqrt{m\, k_h} \tag{6}$$

The wing is modeled as a cantilevered beam that bends and twists. As shown in [15], the natural pulsation corresponding to the first mode of flexural vibration of a cantilever beam is

$$\omega_h = \frac{1.875}{s}\sqrt{\frac{E\, I_x}{A\, \rho}} \tag{7}$$

In addition, from [16], the natural pulsation for the first mode of torsional vibration of a cantilever beam with bi-symmetric sections is given by

$$\omega_\alpha = \frac{\pi}{2\, s}\sqrt{\frac{G\, J}{m\, I_0}} \approx \frac{\pi}{2\, s}\sqrt{\frac{G\, J}{\rho\, I_z}} \tag{8}$$

where I_0, the polar moment of inertia about the shear center is accepted to be $I_0 \approx \frac{I_z}{A}$ (with A the area of the section) since I_x is small and it is assumed the shear center of the section is close to its center of gravity. The torsion constant J is computed as explained in Appendix A.

L and M in Equation 2 are the aerodynamic lift and moment for incompressible, subsonic and inviscid flow. The quasi-steady assumption, used here due to its simplicity, states the at any instant of time, the aerodynamic characteristics of an airfoil with variable linear and angular motion are equal to the aerodynamic characteristics of the same airfoil moving with constant linear and angular velocities equal to the actual instantaneous values [17]. Then the lift and moment become [14]

$$L = \rho\, U^2\, b\left[C_{L\alpha}\left(\alpha + \frac{\dot{h}}{U} + \left(\left(\frac{1}{2} - a\right) b\, \frac{\dot{\alpha}}{U}\right) + C_{L\beta}\,\beta\right]\right. \tag{9}$$

$$M = \rho U^2 b^2\left[C_{M\alpha}\left(\alpha + \frac{\dot{h}}{U} + \left(\left(\frac{1}{2} - a\right) b\, \frac{\dot{\alpha}}{U}\right) + C_{M\beta}\,\beta\right]\right. \tag{10}$$

Finally, $C_{L\beta}$ and $C_{M\beta}$, the lift coefficient and the coefficient of moment of the flap, are modeled using Glauert's theory for a two dimensional airfoil in incompressible fluid [17]

$$C_{L\beta} = \frac{C_{L\alpha}}{\pi}\left(\arccos\left(1 - 2\,EF\right) + 2\sqrt{EF(1-EF)}\right) \tag{11}$$

$$C_{M\beta} = -\frac{C_{L\alpha}}{\pi}\left(1 - EF\right)\sqrt{EF(1-EF)} \tag{12}$$

where $EF = c_f/c$ it the ratio of the flap chord to the total chord. Taking the state vector $x = \begin{bmatrix} h & \alpha & \dot{h} & \dot{\alpha} \end{bmatrix}^T$, a space representation of the system is obtained

$$\dot{x} = A\,x + B\,\beta \tag{13}$$

The fixed parameters of the wing model are summarized in Table 1. The thickness of the flap (t_f) was selected such that the theory for torsion of thin-walled beams applies, i.e. the ratio of width to thickness is higher than 10 [18], whatever the value of EF. Thus t_f depends on the upper bound of the flap proportion EF^{ub}:

$$t_f = \frac{EF^{ub}\,c}{10} \tag{14}$$

Parameter	Value	Unit
c	1.829	m
s	6.096	m
ρ_m	38.2723	kg/m^3
E	1.20625×10^8	N/m^2
G	0.8044×10^7	N/m^2
t_0	0.5	m
t_f	0.0457	m
$C_{L\alpha}$	2π	$1/rad$
$C_{m\alpha}$	0	$1/rad$
ea_b	0.3	-

Table 1: Fixed parameters of the model.

3.1 *Initial design*

- Section with "ghost" flap
  The flap is fixed to 20% of the total chord but $t_f = c_f = 0$. Exterior thickness comply with the thin-walled theory: $t_1 = t_2 = c_s/15$ and $t_3 = t_4 = t_0/15$. Then $t_5 = c_s - 2\,c_s/15$ such as the section is "filled up" as in Fig. 4.

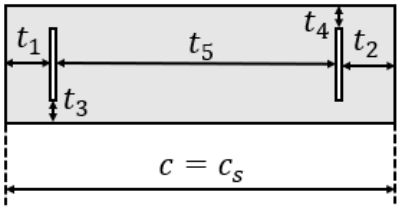

Figure 4: Initial design of the cross-section with the "ghost" flap.

- Section with "real" flap
  Section of Figure 2 is considered. Thicknesses are chosen such that all comply with thin-thickness theory: $t_1 = t_2 = t_5 = c_s/10$ and $t_3 = t_4 = t_0/10$. The flap has mass, t_f is as in Equation 14 and $EF = 0.2$ (or $c_f = 0.2\,c$). In this case EF is a design variable.

3.2 *Open-Loop Analysis*

The initial design for the section with "ghost" flap in open-loop is analyzed. Similar analysis could be done for the "real" flap case. The system has two pairs of complex conjugate poles. From Equations 1, 9 and 10, it can be deduced that the aeroelastic modes and thus the stability of the system depend on the flow speed U. In fact, as long as U increases, the poles move depicting the two branches of Figure 5. The two poles associated with the torsion/pitch mode move to the right half plane and become unstable when the flutter velocity $V_F = 156.7\,m/s$ is reached. Flutter pulsation is $\omega_F = 54.7\,rad/s$. Conversely, plunge/bending poles increase their damping with the increase of the flow speed. It is desired then to increase the speed at which torsion poles become unstable.

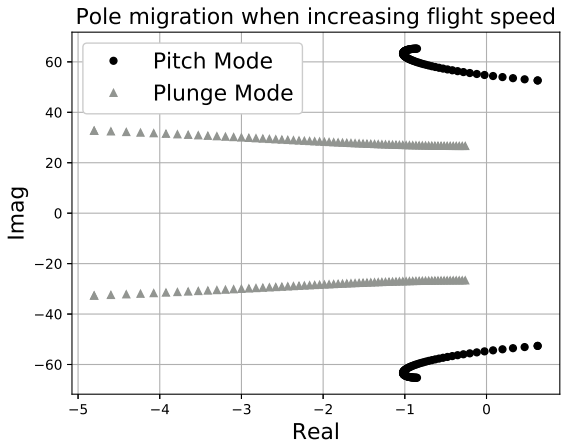

Figure 5: Variation of pole location for the initial design of the cross-section with "ghost" flap in open-loop. As the flow speed increases, the plunge mode (in grey) moves to the left half plane, whereas the pitch mode (in black) moves to the right half plane and becomes unstable at $V_F = 156.7\,m/s$.

4 Control Model

A state feedback controller is used so that the output (the states) of the system is fed back into the input via a controller in the feedback path (Figure 6), thus four gains must be determined. Consequently, the control surface angle (β) is linearly proportional to the velocity ($\dot{h}, \dot{\alpha}$) and displacement (h, α) of the system.

As shown in the previous analysis, the increase of flight speed makes a pair of poles of the aeroelastic system migrate towards the right half plane. Flutter occurs when the poles cross the imaginary axis, i.e. damping is reduced to zero and the structure experiments sustained oscillations. In order to prevent the instability, the controller acts by modifying the behaviour of the system and thus moving the poles back into the left half plane. See in Equation 2 that the proportional gains alter κ and the derivative gains alter ζ, adding extra stiffness and extra damping respectively when the system is in closed-loop [19].

Therefore, the goal of the controller is to stabilize the system at flutter condition and delay it until a

higher speed in order to increase the flight envelope of the aircraft without the increase of its mass.

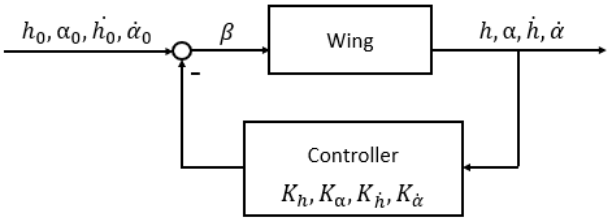

Figure 6: Closed-loop system with the controller on the feedback loop. States are measured and passed through the controller to obtain β. h_0, α_0, $\dot{h}_0$, $\dot{\alpha}_0$ are zero.

5 Optimization

The different optimization problems addressed in this work are summarized in Table 2. Their general expression is as follows

$$\begin{aligned} \min_{\chi} \quad & f(\chi) \\ \text{s.t.} \quad & g(\chi) \geq 0 \\ & lb_\chi \leq \chi \leq ub_\chi \end{aligned} \tag{15}$$

where χ is the vector of design variables, f the objective function, g the flutter inequality constraint, and lb_χ and ub_χ the lower and upper bounds on the design variables. The definition of the inequality constraint is in accordance with the algorithm used, see [20], [21] for further information.

Case	Cross-section	χ	$f(\chi)$
1	"Ghost" flap	t_i, K_i	f_1
2	"Ghost" flap	t_i, K_i	f_2
3	"Real" flap	t_i, K_i, EF	f_2

Table 2: The three optimization problems treated in this work with their cross-section model, design variables and objective function.

5.1 *Design Variables and Bounds*

Ten design variables, composed by both structural and control parameters, are considered.

- The thicknesses $t_i = t_1, t_2, t_3, t_4, t_5$ of the wingbox
- Four feedback gains $K_i = K_h$, K_α, $K_{\dot{h}}$ and $K_{\dot{\alpha}}$ on h, α, $\dot{h}$ and $\dot{\alpha}$, respectively
- The flap proportion $EF = c_f/c$

The bounds on the gains aim to model the saturation of the flap deflection and rate and are set as follows. Suppose flutter makes oscillate the flap with a sinusoidal motion. The input and the rate of input are

$$\beta_{in} = \beta_{max} \sin(2\,\pi\,f_F\,t) \tag{16}$$

$$\dot{\beta}_{in} = \beta_{max}\, 2\,\pi\, f_F\, \cos(2\,\pi\, f_F\, t) \tag{17}$$

with $f_F = \frac{w_F}{2\,\pi}$ the flutter frequency. Assuming a maximum deflection of $\pi/2$, the dynamics of the flap are modeled as

$$\beta_{out} = \frac{\pi}{2} \sin(RL\,t) \tag{18}$$

$$\dot{\beta}_{out} = \frac{\pi}{2}\, RL\, \cos(RL\,t) \tag{19}$$

where RL is the rate limit. In order to provide a satisfactory dynamic response, i.e. to be able to control flutter, the flap must move at least as fast as flutter makes the flap move. Thus the maximum values of equation 17 and 19 become equal to obtain

$$\beta_{max} = \frac{RL}{4\,f_F} \tag{20}$$

Rate limit requirement for civil aircraft is 60 des/s and for military aircraft, 120 deg/s [22]. Goland wing is a very flexible model so RL has to be chosen high to obtain a reasonable value for β_{max}. $RL = 150\,deg/s$ is set.

In closed-loop, the flap deflection is

$$\beta = K_h\, h + K_\alpha\, \alpha + K_{\dot{h}}\, \dot{h} + K_{\dot{\alpha}}\, \dot{\alpha} \tag{21}$$

Considering that h_{max} and θ_{max} are out of phase with respect to $\dot{h}_{max}$ and $\dot{\theta}_{max}$, the previous equation is partitioned into two

$$\begin{aligned} \beta_{max} &\geq K_h\, h_{max} + K_\alpha\, \alpha_{max} \\ \beta_{max} &\geq K_{\dot{h}}\, \dot{h}_{max} + K_{\dot{\alpha}}\, \dot{\alpha}_{max} \end{aligned} \tag{22}$$

Traducing the second equation in the frequency domain

$$\begin{aligned} \beta_{max} &\geq K_{\dot{h}}\, \dot{h}_{max} + K_{\dot{\alpha}}\, \dot{\alpha}_{max} \\ \beta_{max} &\geq K_{\dot{h}}\, s\, h_{max} + K_{\dot{\alpha}}\, s\, \alpha_{max} \\ \beta_{max} &\geq |K_{\dot{h}}\, (j\,\omega_F)\, h_{max} + K_{\dot{\alpha}}\, (j\,\omega_F)\, \alpha_{max}| \\ \frac{\beta_{max}}{\omega_F} &\geq K_{\dot{h}}\ h_{max} + K_{\dot{\alpha}}\, \alpha_{max} \end{aligned} \tag{23}$$

and assuming each term has the same contribution on β_{max}, expressions for the bounds of the gains are obtained

$$\begin{aligned} K_h &= \frac{0.5\,\beta_{max}}{h_{max}} \\ K_\alpha &= \frac{0.5\,\beta_{max}}{\alpha_{max}} \\ K_{\dot{h}} &= \frac{0.5\,\beta_{max}}{\omega_F\, h_{max}} \\ K_{\dot{\alpha}} &= \frac{0.5\,\beta_{max}}{\omega_F\, \alpha_{max}} \end{aligned} \tag{24}$$

Maximum values are set to $h_{max} = 1m$ and $\alpha_{max} = 20\,deg$.

The flap chord is allowed to vary between 10% and 25% of the total chord (ie. $EF^{ub} = 0.25$ and $EF^{lb} = 0.1$).

The upper bounds of t_1, t_2, t_3, t_4 and t_5 are different for the models:

- Section with "ghost" flap

The lower bounds are fixed as follows:

$$\begin{aligned} t_1^{lb} = t_2^{lb} &= \frac{c}{20} \\ t_3^{lb} = t_4^{lb} &= \frac{t_0}{20} \\ t_5^{lb} &= 0 \end{aligned} \tag{25}$$

i.e., the elimination of the central wall. The upper bounds are fixed as follows:

$$\begin{aligned} t_1^{ub} = t_2^{ub} &= \frac{c}{10} \\ t_3^{ub} = t_4^{ub} &= \frac{t_0}{10} \\ t_5^{ub} &= c - \frac{2\,c}{10} \end{aligned} \tag{26}$$

i.e., t_5 can fill all the cross-section. Values are summarized in Table 3.

Lower bound	Design variable	Upper bound
$0.0915\,m$	$t1$	$0.1829\,m$
$0.0915\,m$	$t2$	$0.1829\,m$
$0.0250\,m$	$t3$	$0.0500\,m$
$0.0250\,m$	$t4$	$0.0500\,m$
$0\,m$	$t5$	$1.463\,m$
$-0.0376\,rad/m$	K_h	$0.0376\,rad/m$
-0.1077	K_α	0.1077
$-0.0007\,s/m$	$K_{\dot{h}}$	$0.0007\,s/m$
$-0.0020\,s/rad$	$K_{\dot{\alpha}}$	$0.0020\,s/rad$

Table 3: Bounds on the design variables for the section with "ghost" flap.

- Section with "real" flap

The lower bounds are fixed as follows:

$$\begin{aligned} t_1^{lb} = t_2^{lb} &= \frac{0.9\,c}{20} \\ t_3^{lb} = t_4^{lb} &= \frac{t_0}{20} \\ t_5^{lb} &= 0 \end{aligned} \tag{27}$$

The upper bounds are fixed as follows:

$$\begin{aligned} t_1^{ub} = t_2^{ub} &= \frac{0.9\,c}{10} \\ t_3^{ub} = t_4^{ub} &= \frac{t_0}{10} \\ t_5^{ub} &= \frac{0.9\,c}{10} \end{aligned} \tag{28}$$

since $0.9c$ is the highest value c_s can take, thus the elements of the section can always be considered thin-walled. Values are summarized in Table 4.

Since the design variables belong to different disciplines, and with the aim of making the optimization more homogeneous, the design variables are normalized.

Lower bound	Design variable	Upper bound
$0.0823\,m$	$t1$	$0.1646\,m$
$0.0823\,m$	$t2$	$0.1646\,m$
$0.0250\,m$	$t3$	$0.0500\,m$
$0.0250\,m$	$t4$	$0.0500\,m$
$0\,m$	$t5$	$0.1646\,m$
$-0.0278\,rad/m$	K_h	$0.0278\,rad/m$
-0.0797	K_α	0.0797
$-0.0004\,s/m$	$K_{\dot{h}}$	$0.0004\,s/m$
$-0.0011\,s/rad$	$K_{\dot{\alpha}}$	$0.0011\,s/rad$
0.1	EF	0.25

Table 4: Bounds on the design variables for the section with "real" flap.

5.2 Objective Function

Two different objective functions are considered:

1. $f_1 = \dfrac{m}{m^{OL_{init}}} - \dfrac{V_F^{CL}}{V_F^{OL_{init}}}$
   aims to minimize the mass of the system as well as pushing the flutter boundary as high as possible. Notice the terms are normalized with the mass and flutter speed of the initial design.

2. $f_2 = \dfrac{m}{m^{OL_{init}}}$
   aims to minimize the mass of the system (the flutter speed requirement is introduced in the constraints).

5.3 Algorithm

In all the cases, SLSQP (Sequential Least Squares Quadratic Programming) of SciPy Python package [23], [24], a gradient-based algorithm, has been used. Sequential quadratic programming is the most efficient programming method to solve nonlinear optimization problems under equality and inequality constraints and bounds on the variables [21]. The numerical approximation of the Jacobian is obtained using a 2-point finite difference estimation with a step size of 0.05. The tolerance for termination tol_f is set to 1×10^{-4}.

5.4 Flutter Constraint

A flutter constraint is enforced in order to avoid the degradation of the flutter speed of the system with the reduction of mass. The flutter speed of the system operating in closed-loop (V_F^{CL}) is ensured to be at least equal to flutter speed of the initial open-loop system ($V_F^{OL_{init}}$).

$$g(\chi) = \frac{V_F^{CL}}{V_F^{OL_{init}}} - 1 \geq 0 \tag{29}$$

The flutter speed of the system (either in open or closed-loop) is computed with the classic *V-g method*: the damping factor of the poles of the system is computed at different flow speeds and the speed for which the damping factor is zero, corresponds to the flutter speed. A step size of $\Delta U = 0.1\ m/s$ is considered.

Computational efficiency increases with the decrease of the step size ΔU.

It is essential to remark the importance of choosing ΔU small enough in comparison with the step size used for the numerical approximation of the Jacobian of the optimizer (ε).

As explained in [21], the search direction (d) of the algorithm is determined by a quadratic programming sub-problem (Equation 30) formulated by a quadratic approximation of the Lagrange function (Equation 31) and linear approximation of the constraints of the problem.

$$\begin{aligned} \min_{d \epsilon R^n} \quad & \frac{1}{2}\, d\, \nabla^2_{xx} L(\chi, \lambda)\, d \;+\; \nabla f(\chi^k)\, d \\ \text{s.t.} \quad & \nabla g(\chi^k)\, d + g(\chi^k) \geq 0 \end{aligned} \tag{30}$$

$$L(\chi, \lambda) = f(\chi) - \lambda\, g(\chi) \tag{31}$$

Therefore, the search direction depends on $\frac{\partial f}{\partial \chi}(\chi^k)$, $\frac{\partial^2 f}{\partial \chi^2}(\chi^k)$ and $\frac{\partial^2 g}{\partial \chi^2}(\chi^k)$. The derivatives are approximated as follows

$$\frac{\partial f}{\partial \chi}(\chi^k) = \frac{f(\chi^k + \varepsilon) - f(\chi^k)}{\varepsilon} \tag{32}$$

$$\frac{\partial g}{\partial \chi}(\chi^k) = \frac{g(\chi^k + \varepsilon) - g(\chi^k)}{\varepsilon} \tag{33}$$

If $\varepsilon \ll \Delta U$, the flutter speed is the same for χ_c and for $\chi_c + \varepsilon$ causing $\partial f / \partial \chi_c$ and $\partial g / \partial \chi_c$ to be zero. As a result, control design variables (χ_c) do not move during the optimization. Nevertheless, as ε increases, the precision of the optimal solution decreases. In this work, $\varepsilon = 0.05$ has been chosen.

6 Results and Discussion

6.1 *Co-design improvement over sequential design*

Co-design is performed for *Case 1* and compared with a sequential design: first the optimal structural parameters are obtained and then the controller is optimized. Results are compared in Table 5. The former converges to lower structural weight due to the reduction of mass in t_5. To satisfy the flutter constraint, K_h and $K_{\dot{h}}$ are increased.

The signs of the gains are explained as follows. The states of the system are measured and then passed through the controller to directly obtain β (since reference values are all zero) and fed back into the system. A positive α of the system means it is pitching up (see Figure 3) and to go back to $\alpha = 0$ the system has to pitch down, thus the flap must generate a force upwards through a positive deflection β (downwards). If α and β are positive, and considering $\beta = K_\alpha\, \alpha$, K_α has to be positive. Same reasoning applies for $K_{\dot{\alpha}}$. A positive h of the system means it is plunging down (see Figure 3), thus to reach $h = 0$, it has to go up producing more lift and a negative h through a positive flap deflection. Therefore, considering $\beta = K_h\, h$, K_h has to be negative. Same reasoning applies for $K_{\dot{h}}$.

Variable	Co-design	Sequential design
$t1$	$0.1829\, m$	$0.1829\, m$
$t2$	$0.0915\, m$	$0.0915\, m$
$t3$	$0.0500\, m$	$0.0500\, m$
$t4$	$0.0500\, m$	$0.0500\, m$
$t5$	$0.4121\, m$	$0.6154\, m$
K_h	$-0.0100\, rad/m$	$0\, rad/m$
K_α	0.1077	0.1077
$K_{\dot{h}}$	$-0.0007\, s/m$	$0\, s/m$
$K_{\dot{\alpha}}$	$0.0020\, s/rad$	$0.0020\, s/rad$
Mass	$106.7\, kg$ (50.0%)	$125.7\, kg$ (58.9%)
V_F^{CL}	$156.8\, m/s$	$169.8\, m/s$

Table 5: Optimal values of the design variables, mass and flutter velocity in closed-loop for *Case 1* obtained through sequential design and co-design. Being the mass of the initial design $213.4\, kg$, sequential optimal design weights 58.9% of the initial design, whereas co-design optimal design weights 50% of the initial design. Thus, co-design produces a higher mass reduction.

.

6.2 *Maintaining or improving flutter performance*

Case 1 and *Case 2* of Table 2 are compared. The objective function of *Case 2* aims reducing the mass, whereas the objective function of *Case 1* aims reducing the mass of the system as well as maximizing the flutter speed. Results obtained with both objective functions are the same (those displayed in the Co-design column of Table 5). The bounds on the gains K_α and $K_{\dot{\alpha}}$ are already reached for *Case 2* in order fulfill the flutter constraint, thus the only way to increase V_F^{CL} in *Case 1* would be by increasing the mass of the system. However, since the minimization of the mass is also considered in the objective function, the mass is not increased and results are the same in both cases. It is clearly seen here the saturation of flap deflection and rate put the limit on how far the flutter condition can be pushed. From this comparison it is deduced that for the initial design treated here, the objective function f_2 can be considered. f_2 complies better with the design procedure of an aircraft, where the velocity the structure can flutter at is previously defined and the main interest is to minimize the mass of the structure. However, f_1 with weights in the terms or even f_1 for other initial designs should not be dismissed. The choice of the objective function depends on the judgment of the designer.

6.3 *Co-design of a thin walled section*

Case 3 of Table 2 outputs a reduction of 20.25% of the mass of the wing while maintaining the initial flutter velocity $V_F = 139\, m/s$. The optimal size of the flap is 20.03% of the total chord. The optimal values of the gains and thicknesses are shown in Table 6 and their evolution in the optimization is shown in Figure 10. Also in Table 6 the obtained optimal values are compared with those if $t_f = \frac{EF^{ub}\, c}{12}$ was selected, to show the optimal design is dependant on the thickness given

to the flap. If the flap is thinner, as the objective is to reduce the mass of the system, the optimizer makes the flap bigger: it is more convenient to increase the flap portion (that increases the aerodynamic effect of the flap and thus the flutter velocity in closed-loop) than the wingbox portion (that increases the flutter velocity in open-loop by adding mass).

Design variable	$t_f = \frac{EF^{ub}\, c}{10}$	$t_f = \frac{EF^{ub}\, c}{12}$
$t1$	$0.1394\, m$	$0.1394\, m$
$t2$	$0.0823\, m$	$0.0823\, m$
$t3$	$0.0500\, m$	$0.0500\, m$
$t4$	$0.0500\, m$	$0.0500\, m$
$t5$	$0.0458\, m$	$0.0435\, m$
K_h	$-0.0127\, rad/m$	$-0.0112\, rad/m$
K_α	0.0797	0.0784
$K_{\dot{h}}$	$-0.0004\, s/m$	$-0.0004\, s/m$
$K_{\dot{\alpha}}$	$0.0006\, s/rad$	$0.0006\, s/rad$
EF	0.2003	0.2058

Table 6: Optimal values depend on the thickness given to the flap.

The flutter velocity in closed loop is slightly affected when varying K_h, thus this design variable slightly moves. In fact, since the plunge mode is stable and K_h affects the stiffness (and not the damping) of the system, it is a coherent result. Figure 7 shows the pole migration when increasing speed of the final design in open and closed-loop to point out the effect of the controller. Indeed, Figure 8 shows the potential of co-design: the flutter speed of the open-loop is relaxed through the reduction of the mass of the system and the controller works increasing the flutter velocity of the system in closed-loop.

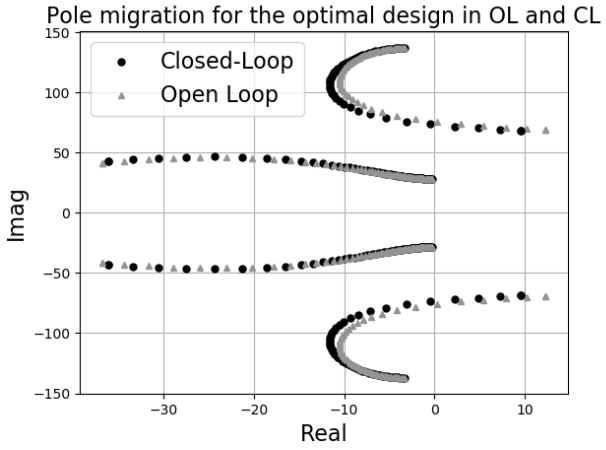

Figure 7: Pole migration when increasing speed for the optimal design in open loop (in grey) and in closed-loop (in black). See poles are moved to the left half side thus flutter occurs at higher speeds.

6.4 Robustness analysis

It is intended to asses the robustness of the controller to variations on the thicknesses of the cross-section.

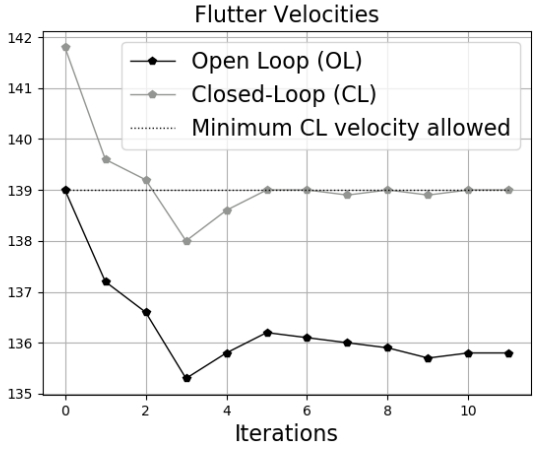

Figure 8: Evolution of the flutter velocity in open and closed-loop throughout the optimization iterations. The minimum closed-loop allowed velocity, which corresponds to the open loop velocity of the initial design, is also shown. The flutter speed of the open-loop is relaxed through the reduction of the mass of the system and the controller works increasing the flutter velocity of the system in closed-loop. See the optimizer is allowed to disregard the constraints in some iterations (as in iteration 4 for example) in order to explore new regions of the design space and attempt to find more optimal solutions ([21] provides further information).

Considering *Case 3*, it is found the system becomes unstable if the thicknesses are only 4% lower than the optimal ones (Figure 9). Thus, the design lacks of robustness.

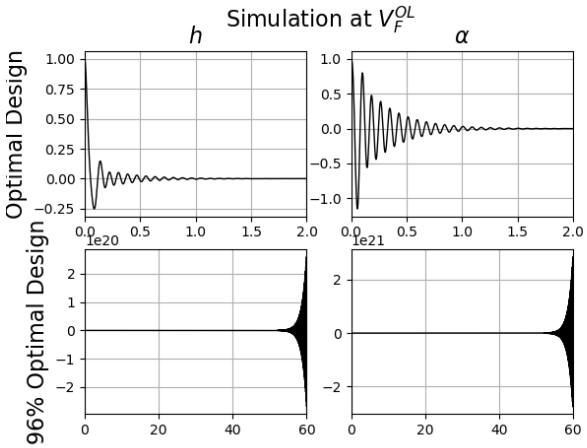

Figure 9: Simulation of the optimal design and a design with thicknesses slightly reduced (96% of the optimal) at V_F^{OL} of the optimal design. The latter is unstable. The design is not robust to thicknesses variations.

7 Conclusions

The capability of co-design method to relax the open loop flutter velocity and attain lighter designs was explored through the test of different models, objective functions and design variables. Despite the limitations of SciPy, it was possible to perform the optimization of ten design variables of the structure and control sys-

tem. Co-design has shown to achieve important mass reductions. However, a state-feedback controller did not succeed in providing a robust design.

8 Future Work

The following steps are proposed to continue with this work:

- Consider different control techniques, in particular those assuring robustness such as H_{inf} or LQR.
- A stress based analysis must be introduced to make the co-design more realistic. For instance, top and down horizontal thickness of the cross-section were obtained equal (Fig. 10e). However, since lift makes wings bend up, the top wall is in compression and the lower one in tension. Thus, the top wall must be larger to avoid buckling. Stress constraints can be added to the optimization as explained in [25].
- The numerical issue described in 5.4 was solved by increasing ε at the expense of losing precision on the optimal solution. A better alternative would be to increase ε of the control design variables only. However, this is not possible with SciPy (but it is in OpenMDAO). Then moving to OpenMDAO is a preferred solution. A second alternative is to test the use the complex-step-finite-difference method explained in [26].
- The aeroelastic model used here leaves room for improvement. Some propositions are: using unsteady aerodynamics and the *p-k method* [27] to determine flutter condition, find more accurate models for the torsional constant for sections containing both, solid and thin elements, or better model the mass and structure of the flap. It will be also interesting to make the position of the elastic axis of the cross-section vary since it has a direct influence on flutter velocity [28].

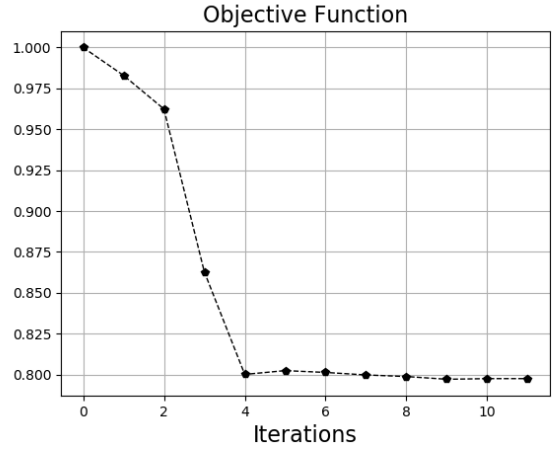

(a) The objective function, $f = f_2 = \frac{m}{m^{OL_{init}}}$ indicates a 20.25% of mass reduction with respect to the initial design.

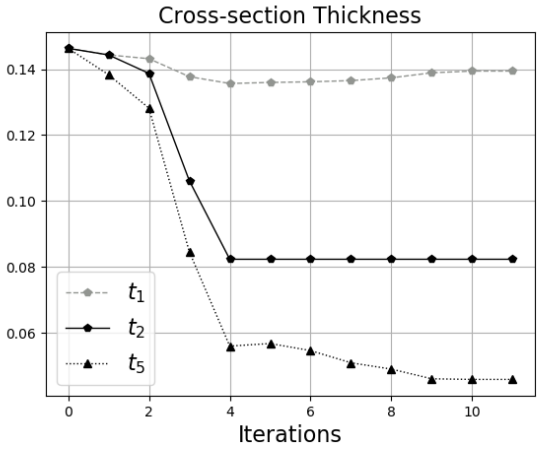

(b) Vertical thicknesses t_1, t_2, t_5.

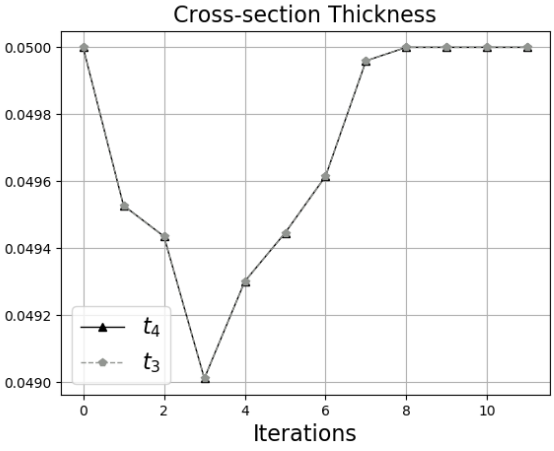

(c) Horizontal thicknesses t_3, t_4. t_3 and t_4 are overlapped.

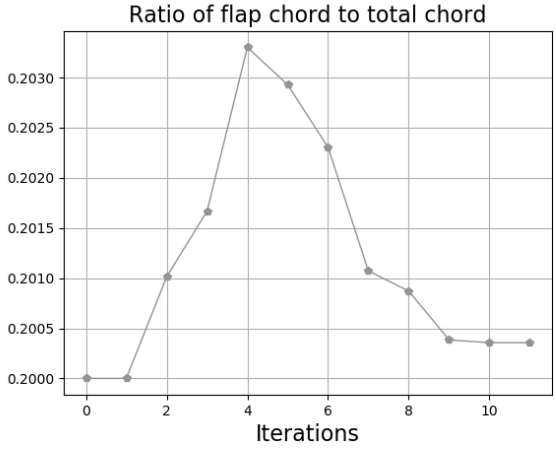

(d) EF: ratio flap chord (c_f) to total chord (c).

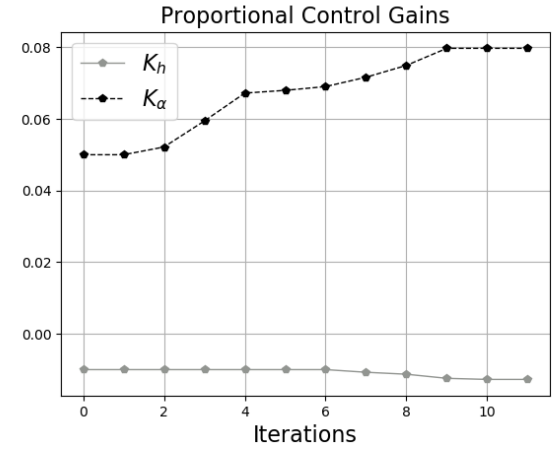

(e) Proportional control gains K_h and K_α.

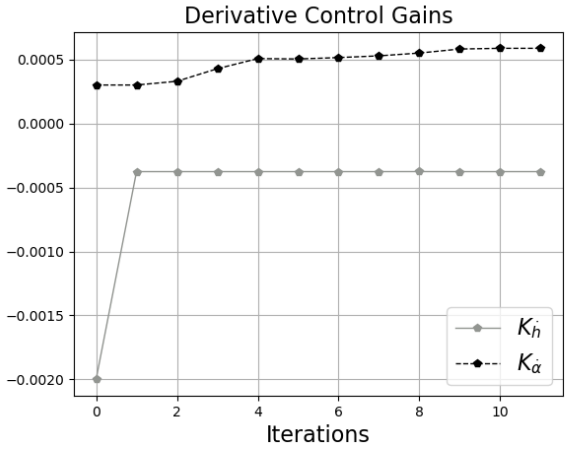

(f) Derivative control gains $K_{\dot{h}}$ and $K_{\dot{\alpha}}$.

Figure 10: Evolution of the objective function and the design variables throughout the optimization iterations for *Case 3*.

A Torsion constant

The torsion constant of the cross-section of Figure 2 is obtained considering the thin-walled theory [29] and the torsion constant of a rectangular element with different thickness to width ratio [30]. All the thicknesses are considered to be thin, except t_5 that may be not.

If t_5 is thin (as for the cross-section with "real" flap), then J is the sum of the torsional constant of a thin-walled two-cell closed section (J_{tw2}) and a thin rectangular element (the flap) (J_f): $J = J_{tw2} + J_f$.

$$J_{tw2} = 4\,(\frac{c_s}{2}\,t_0)^2\,\frac{I_{22} + I_{11} - I_{12}}{I_{11}\,I_{22} - I_{12}^2} \tag{34}$$

With

$$I_{11} = t_0/t_1 + t_0/t_5 + c_s/(2\,t_3) + cs/(2\,t_4)$$
$$I_{22} = t_0/t_2 + t_0/t_5 + c_s/(2\,t_3) + cs/(2\,t_4)$$

$$I_{12} = -t_0/t_5$$

$$J_f = \frac{c_f\,t_f^3}{3} \tag{35}$$

If t_5 is not thin (as for the cross-section with "ghost" flap), then J is the sum of the torsional constant of a thin-walled one-cell closed section (J_{tw1}) and a rectangular solid element - the middle tab- (J_5): $J = J_{tw1} + J_5$.

$$J_{tw1} = \frac{4\,(c_s\,t_0)^2}{t_0/t_1 + h/t_2 + c_s/t_3 + c_s/t_4} \tag{36}$$

$$J_5 = \frac{l\,s^3}{3} - \Phi\,s^4 \tag{37}$$

Where l is the longest side of the tab, s, the shortest and Φ is the coefficient extracted from Figure 11.

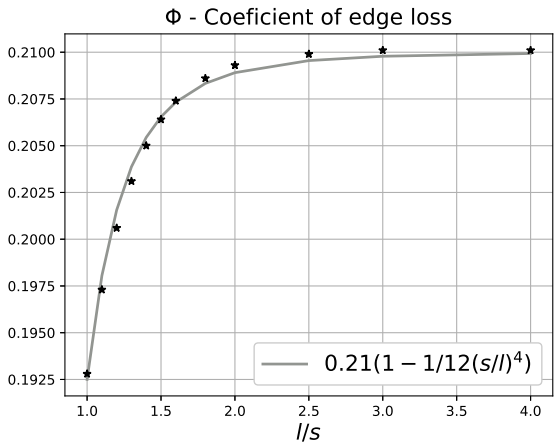

Figure 11: Coefficient of edge loss for a rectangular cross section as funciton of the ratio of its two dimensions: l, the long side and s, the short side. Data is taken from [30].

Models are compared in Figure 12, where the torsion constant of the section if it was all solid is also included as reference.

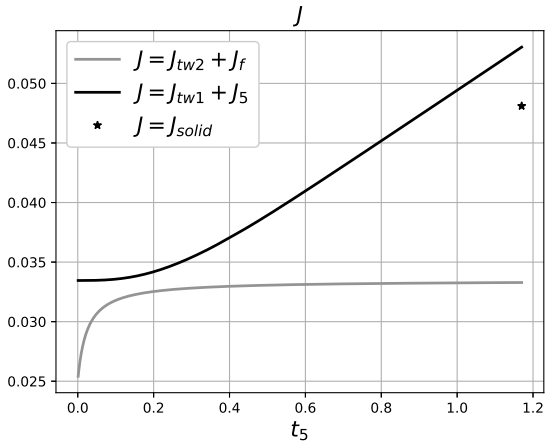

Figure 12: Models to estimate the torsion constant as function of t_5. The other thicknesses are those of the initial designs described in 3.1. The gray model considers a two-cell thin-walled cross-section and a thin element for the flap. The black model considers a one-cell thin-walled cross-section and wide element for the middle tab. For reference, it is added the value of the torsion constant if the cross-section was solid.

B Structural Damping

The modelling of structural damping is complex and unclear. Thus, any model guaranteeing the dissipation rate is non-negative is a good candidate [31]. For the baseline model used in this work, damping ratios of 1% of the critical damping for each mode can be considered [19]. This damping corresponds to the viscous structural damping that is supposed to be determined only by the instantaneous generalized velocities. The equations of motions for free vibration of each mode are

$$I_\alpha\,\ddot{\alpha} + c_\alpha\,\dot{\alpha} + k_\alpha\,\alpha = 0 \tag{38}$$

$$m\,\ddot{h} + c_h\,\dot{h} + k_h\,h = 0 \tag{39}$$

The critical damping (cd) is

$$cd_\alpha = \sqrt{4\,I_\alpha\,k_\alpha} \tag{40}$$

$$cd_h = \sqrt{4\,m\,k_h} \tag{41}$$

Therefore

$$c_\alpha = 0.01\,cd_\alpha = 0.02\,\sqrt{I_\alpha\,k_\alpha} \tag{42}$$

$$c_h = 0.01\,cd_h = 0.02\,\sqrt{m\,k_h} \tag{43}$$

References

[1] P. P. Friedmann, Renaissance of aeroelasticity and its future, *Journal of aircraft* **36**, 105 (1999).

[2] T. H. G. Megson, *Aircraft structures for engineering students* (Elsevier, 2007).

[3] M. A. Shubov, Mathematical modeling and analysis of flutter in bending-torsion coupled beams, rotating blades, and hard disk drives, *Journal of Aerospace Engineering* **17**, 56 (2004).

[4] M. A. Shubov, Flutter phenomenon in aeroelasticity and its mathematical analysis, *Journal of Aerospace Engineering* **19**, 1 (2006).

[5] E. Livne, Aircraft active flutter suppression: State of the art and technology maturation needs, *Journal of Aircraft* **55**, 410 (2018).

[6] J. T. Allison, T. Guo, and Z. Han, Co-design of an active suspension using simultaneous dynamic optimization, *Journal of Mechanical Design* **136** (2014).

[7] H. Asada, J.-H. Park, and S. Rai, in *Proceedings. 1991 IEEE International Conference on Robotics and Automation* (IEEE Computer Society, 1991), 2356–2357.

[8] E. N. Van, D. Alazard, C. Döll, and P. Pastor, Co-design of aircraft vertical tail and control laws using distributed electric propulsion, *IFAC-PapersOnLine* **52**, 514 (2019).

[9] R. HAFTKA, in *Dynamics Specialists Conference* (1990), 1190.

[10] S. S. Rao, Combined structural and control optimization of flexible structures, *Engineering Optimization* **13**, 1 (1988).

[11] B. K. Stanford, Optimization of an aeroservoelastic wing with distributed multiple control surfaces, *Journal of Aircraft* **53**, 1131 (2016).

[12] E. Faïsse, R. Vernay, F. Vetrano, D. Alazard, and J. Morlier, in *AIAA Scitech 2021 Forum* (2021), 0892.

[13] B. Raghavan and M. J. Patil, Flight dynamics of high aspect-ratio flying wings: effect of large trim deformation, *Journal of Aircraft* **46**, 1808 (2009).

[14] J. Ko, A. Kurdila, and T. Strganac, in *35th Aerospace Sciences Meeting and Exhibit* (1997), 580.

[15] W. F. Stokey, in *Harris' Schock and Vibration Handbook*, edited by C. M. Harris and A. G. Piersol (McGRAW-HILL, 2002), chap. 7, 5th ed.

[16] W. Jrad, Ph.D. thesis, Université de Lorraine (2019).

[17] Y. C. Fung, *An introduction to the theory of aeroelasticity* (Courier Dover Publications, 2008).

[18] J. N. G. S. Timoshenko, *Theory of elasticity* (McGraw-Hill Book Company, Inc., 1951).

[19] J. R. Wright and Cooper, *Introduction to aircraft aeroelasticity and loads* (John Wiley & Sons, 2015).

[20] Optimization (scipy.optimize), https://docs.scipy.org/doc/scipy/reference/tutorial/optimize.html.

[21] D. Kraft et al., A software package for sequential quadratic programming (1988).

[22] J.-J. Charrier and A. Kulshreshtha, in *45th AIAA Aerospace Sciences Meeting and Exhibit* (2007), 1391.

[23] scipy.optimize.minimize, https://docs.scipy.org/doc/scipy/reference/generated/scipy.optimize.minimize.html#scipy.optimize.minimize.

[24] minimize(method='slsqp'), https://docs.scipy.org/doc/scipy/reference/optimize.minimize-slsqp.html.

[25] A. B. Lambe, G. J. Kennedy, and J. R. Martins, An evaluation of constraint aggregation strategies for wing box mass minimization, *Structural and Multidisciplinary Optimization* **55**, 257 (2017).

[26] R. Abreu, D. Stich, and J. Morales, The complex-step-finite-difference method, *Geophysical Journal International* **202** (2015).

[27] H. J. Hassig, An approximate true damping solution of the flutter equation by determinant iteration., *Journal of Aircraft* **8**, 885 (1971).

[28] S. Huo, F. Wang, Z. Yuan, and Z. Yue, Composite wing elastic axis for aeroelasticity optimization design, *Aircraft Engineering and Aerospace Technology* (2013).

[29] V. Lubarda, On the torsion constant of multicell profiles and its maximization with respect to spar position, *Thin-walled structures* **47**, 798 (2009).

[30] C. F. Kollbrunner and K. Basler, *Torsion in structures: an engineering approach* (Springer Science & Business Media, 2013).

[31] V. Arora, Structural damping identification method using normal frfs, *International Journal of Solids and Structures* **51**, 133 (2014).

Declaration of Authenticity

This assignment is entirely my own work. Quotations from literature are properly indicated with appropriated references in the text. All literature used in this piece of work is indicated in the bibliography placed at the end. I confirm that no sources have been used other than those stated. I understand that plagiarism (copy without mentioning the reference) is a serious examinations offence that may result in disciplinary action being taken.